Chinese Chemical Letters 36 (2025) 110057

Contents lists available at ScienceDirect

Chinese Chemical Letters

journal homepage: www.elsevier.com/locate/cclet

Cation-π enhanced triplet-to-singlet Förster resonance energy transfer for fluorescence afterglow

Shuai Qiu[a,b], Jia He[a], Xiao Hu[a], Hongxia Yan[a], Zhao Gao[a], Wei Tian[a,*]

[a] Shaanxi Key Laboratory of Macromolecular Science and Technology, Xi'an Key Laboratory of Hybrid Luminescent Materials and Photonic Device, MOE Key Laboratory of Material Physics and Chemistry under Extraordinary Conditions, School of Chemistry and Chemical Engineering, Northwestern Polytechnical University, Xi'an 710072, China

[b] Engineering Research Center for Nanomaterials, Henan University, Kaifeng 475004, China

ARTICLE INFO

Article history:
Received 11 March 2024
Revised 15 May 2024
Accepted 26 May 2024
Available online 27 May 2024

Keywords:
Triplet-to-singlet Förster resonance energy transfer
Cation-π interaction
Dipole-dipole interaction
Fluorescence afterglow

ABSTRACT

The construction of triplet-to-singlet Förster resonance energy transfer (TS-FRET) systems has significantly contributed to the advancement of high-performance optoelectronic materials, particularly in the development of metal-free organic environmental afterglow materials. Despite these notable advancements, achieving highly efficient energy transfer between luminescent donor and acceptor molecules remains a formidable challenge. In this study, we present the utilization of cation-π interactions as an effective strategy to enhance TS-FRET efficiency, with the ultimate objective of further advancing fluorescence afterglow materials. Our results demonstrate that the cation-π interaction in 1D supramolecular nanorods (1D-SNRs) enhances the dipole-dipole coupling, a crucial parameter for regulating TS-FRET between the triplet state phosphorescent donor and singlet state fluorescent acceptor. As a result, we achieved an outstanding TS-FRET efficiency of up to 97%. Furthermore, the 1D-SNRs exhibit a long-lifetime afterglow property, which suggests their potential application as a cost-effective and secure medium for information encryption. Thus, our findings highlight the promising prospects of cation-π interactions in enhancing TS-FRET efficiency and advancing the field of organic photo-functional materials.

Förster resonance energy transfer (FRET) is a distance-dependent nonradiative process mediated by long-range dipole-dipole interactions. It involves the transfer of energy from an excited donor to a ground-state acceptor. This phenomenon has found extensive applications in chemical analysis, biosensors and imaging, energy harvesting, photocatalysis, and light-emitting materials, owing to its high sensitivity [1–8]. One innovative and promising energy transfer methodology is the triplet-to-singlet FRET (TS-FRET), where energy is transferred from an excited donor phosphor in its triplet state to the singlet state of the acceptor. TS-FRET offers a fast transition rate and exceptional material properties, making it of great interest, especially in the context of organic fluorescence afterglow materials [9–11]. However, the efficiency of TS-FRET systems is often limited by the random arrangement of the donor and acceptor molecules, leading to suboptimal energy transfer efficiency [12,13]. To advance many optoelectronic devices, it is crucial to increase and control TS-FRET efficiency [14]. Nevertheless, achieving high-efficiency TS-FRET systems remain a fascinating yet challenging issue. Thus, there is a need for a simple approach to overcome this limitation and enhance TS-FRET efficiency effectively.

Until now, several excellent strategies have been reported to achieve TS-FRET systems, such as doping systems, crystal forms, molecular engineering, supramolecular complexation, and polymerization [15–23]. However, these strategies rely on achieving suitable distances and spectral overlap between the energy donor and acceptor. Additionally, the efficiency of TS-FRET is influenced by key parameters, including the radiative emission rate of the donor, the relative orientation (k^2), and the dipole-dipole interaction between the donor and acceptor, as per Förster theory [24,25]. Of particular importance is the dipole-dipole interaction, acting as a bridge between the donor and acceptor in the spin angular momentum space, especially when either the donor or acceptor chromophore possesses an anisotropic dipole state [26,27]. Regrettably, most reported TS-FRET systems suffer from weak dipole-dipole coupling interactions, resulting in inefficient energy transfer due to insufficient intersection of the spin angular momentum space formed by the ground and excited states of the donor and acceptor. Thus, the development of a new strategy to enhance the dipole-dipole interaction for efficient TS-FRET is

* Corresponding author.
E-mail address: happytw_3000@nwpu.edu.cn (W. Tian).

https://doi.org/10.1016/j.cclet.2024.110057
1001-8417/

of utmost importance, not only from a fundamental perspective but also to provide innovative ideas for the advancement of fluorescence afterglow materials.

The ion-π interaction, which involves anions/cations and aromatic groups in a non-covalent manner, has been extensively studied for its crucial role in various biological and photochemical processes [28–30]. Specifically, the cation-π interaction, a subtype of ion-π binding force occurring between positively charged cations and electron-rich π systems, is known to be one of the strongest non-covalent interactions [31–35]. Furthermore, it can be modulated by off-axis interactions, allowing for well-defined control over the interaction distance and strength. Considering these characteristics, it is reasonable to speculate that the cation-π interaction could be leveraged to develop efficient TS-FRET systems, and the following factors support this notion. Firstly, the cation-π interaction induces an uneven distribution of the electron cloud between the donor and acceptor, resulting in a greater dipole moment. This, in turn, enhances the dipole-dipole interaction between the donor and acceptor, facilitating efficient energy transfer [36]. Secondly, during the self-assembly process, the cation-π interaction enables precise control over the orientation of donor-acceptor dipole moments, leading to an organized structure and excellent fluorescence afterglow properties.

Building upon our previous research [37], we propose a novel approach to constructing an efficient TS-FRET system by utilizing cation-π interactions to enhance dipole-dipole interactions and adjust donor-acceptor geometrical orientation (Fig. 1). To achieve this, we employed a C_3-symmetric monomer Trz-$(Cbz)_3$ containing a triazine group and three carbazole arms as the triplet state donor. As the representative singlet state acceptor chromophore, we used Rhodamine 6G (Rh6G), a commercially available cationic dye. Through the strategic use of cation-π interactions between the N^+ in the quaternary ammonium group of Rh6G and the carbazole in Trz-$(Cbz)_3$, we successfully constructed 1D supramolecular nanorods (1D-SNRs) with well-ordered structures (Fig. 1a). These 1D-SNRs exhibited significantly enhanced dipole-dipole interactions between Trz-$(Cbz)_3$ and Rh6G, resulting in a remarkable TS-FRET efficiency of 97% between the donor and acceptor (Fig. 1b). In addition to their efficient TS-FRET properties, the 1D-SNRs displayed afterglow luminescence with a lifetime of 226 ms and a quantum yield of approximately 16.6% at 608 nm under ambient conditions. These exceptional characteristics of 1D-SNRs based on RTP materials, along with the efficient TS-FRET system,

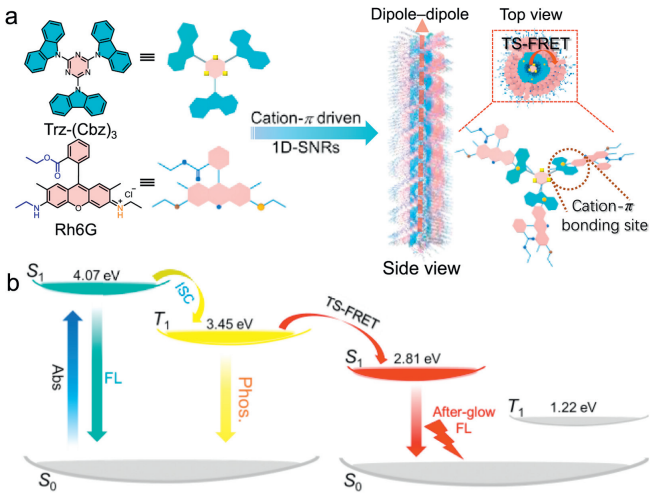

Fig. 1. Schematic illustration of the formation process of 1D SNRs and their TS-FRET mechanism diagram. (a) Cation-π interaction driven the formation of 1D-SNRs. (b) Simplified Jablonski diagram to explain the process of TS-FRET.

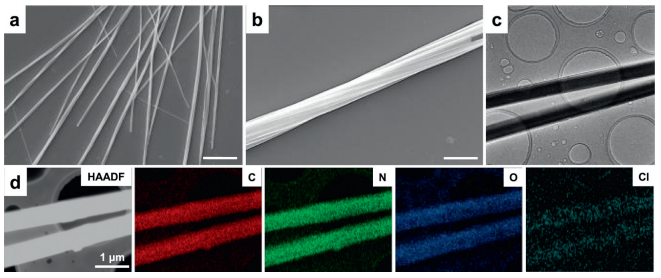

Fig. 2. Morphology characterization of the obtained 1D-SNRs. (a, b) SEM images showing the solid nanorods structures with various magnifications. (c) TEM, (d) HAADF-STEM images and corresponding EDS-mapping images of 1D-SNRs.

indicate their potential applications as cost-effective and secure materials for information encryption.

In Fig. 1a, we present the desired triplet state phosphorescent donor, Trz-$(Cbz)_3$, and the singlet state fluorescent acceptor, Rh6G. Trz-$(Cbz)_3$ is comprised of three sets of symmetrical carbazolyl groups linked on the periphery of the cyanuric unit (Scheme S1 in Supporting information). Notably, these three carbazolyl groups serve as both phosphorescent groups and provide the necessary π moiety to interact with the commercially available dye, Rh6G, which exhibits strong cation-π interaction with the donor, the cation-π can induce the non-uniform distribution of the donor-acceptor electron cloud and enhance the dipole-dipole interaction between them. Detailed synthetic procedures and characterization results of the two monomers are provided in Supporting information and the purity of the Trz-$(Cbz)_3$ was verified by HPLC (Fig. S1 in Supporting information).

The 1D-SNRs were prepared using a solution co-assembly method (Section 3 in Supporting information). To characterize their morphology, scanning electron microscopy (SEM), transmission electron microscopy (TEM), high-angle annular dark-field scanning transmission electron microscopy (HAADF-STEM), and energy-dispersive X-ray spectroscopy (EDS) were employed. The SEM and TEM images revealed the formation of 1D-SNRs with straight, uniform width (approximately 600 nm), and randomly oriented structures (Figs. 2a-c). Most 1D-SNRs exhibited lengths of several micrometers, with smooth surfaces and right-handed superhelices throughout their entire length. Although no chiral signals were detected, it is likely that the inability to control the system's chirality during the assembly process led to this observation (Fig. S3 in Supporting information). The HAADF-STEM and EDS results provided evidence that the 1D-SNRs were solid nanorods with a uniform distribution of C, N, O, and Cl elements throughout their entire structure (Fig. 2d). In comparison, when Trz-$(Cbz)_3$ was self-assembled independently, only thin nanofibers with a width of about 200 nm were observed, and the aggregates of Rh6G formed three-dimensional blocky structures (Fig. S2 in Supporting information). This indicates that no similar nanorods were observed in the individual self-assemblies of the two monomers. Consequently, the co-assembly of Trz-$(Cbz)_3$ and Rh6G resulted in the formation of 1D-SNRs with compact, uniform, and ordered structures.

Understanding the photophysical properties of the donor (Trz-$(Cbz)_3$) and acceptor (Rh6G) is crucial for studying the TS-FRET processes in 1D-SNRs. In the solid state, the fluorescence emission spectrum of Trz-$(Cbz)_3$ solid powders showed a strong emission peak at 452 nm with 43% fluorescence quantum yield and 153 ns lifetime under 365 nm irradiation (Figs. S4a and b in Supporting information). Interestingly, excitation-phosphorescence mapping revealed phosphorescent emission peaks at 554 nm with lifetimes of 232 ms (Figs. 3a and b), confirming its RTP emission characteristics. After removing the UV light source, a significant yellow long afterglow emission was observed (Fig. S5 in Support-

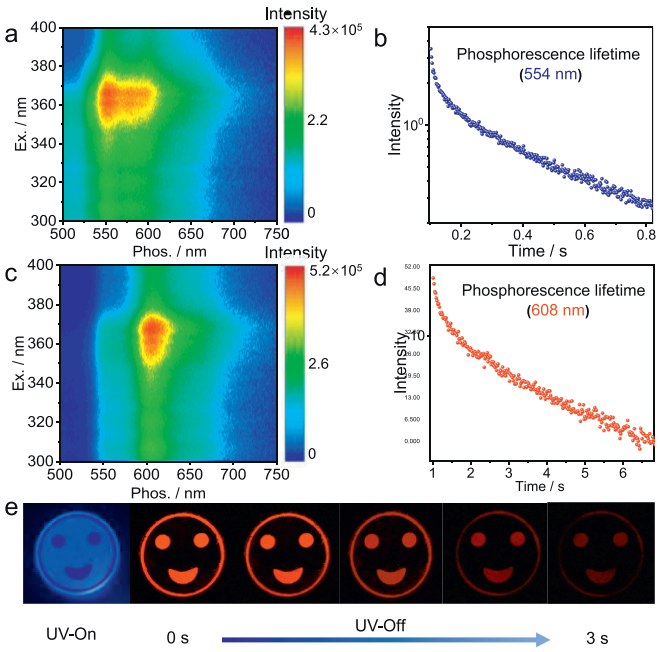

Fig. 3. Photophysical properties of Trz-$(Cbz)_3$ and 1D-SNRs. (a) Excitation-phosphorescence mapping and (b) lifetime decay profiles of Trz-$(Cbz)_3$ at 554 nm. (c) Excitation-phosphorescence mapping and (d) long-life fluorescence decay lifetimes of 1D-SNRs (the ratio of D/A is 5:1) at 608 nm. (e) Luminescence photos of 1D-SNRs powders under UV light irradiation at 365 nm and at different time intervals after removing the UV light.

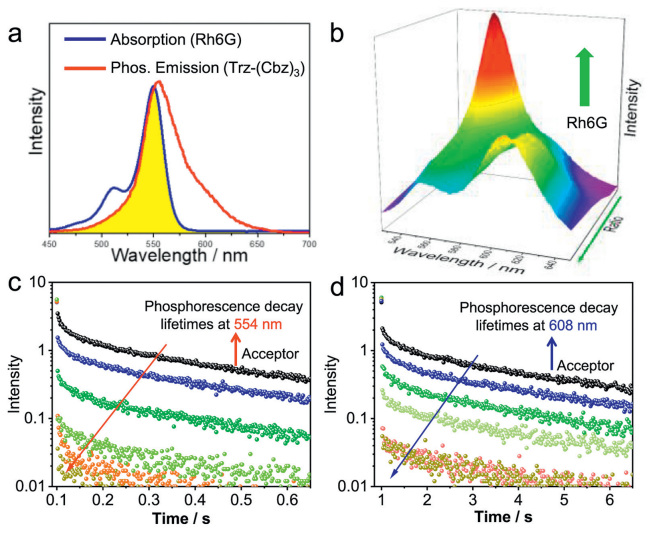

Fig. 4. TS-FRET studies of 1D-SNRs. (a) Absorption spectrum (blue line) of Rh6G and delayed emission (red line) spectrum of Trz-$(Cbz)_3$. (b) Delayed emission spectra of 1D-SNRs solid powder at different ratios of Trz-$(Cbz)_3$ and Rh6G (delay time = 5 ms) (λ_{ex} = 328 nm). (c, d) Lifetime decay plot of 554 nm and 608 nm of 1D-SNRs solid powders with different ratios of Trz-$(Cbz)_3$ and Rh6G showing a quenching of the Trz-$(Cbz)_3$ triplet lifetime with increasing percentage of Rh6G.

ing information). The small energy gap between S_1 and T_n was thought to enhance the intersystem crossing (ISC) process, thus generating the phosphorescent properties of Trz-$(Cbz)_3$. Surprisingly, in the excitation-phosphorescence mapping of the 1D-SNRs solid powders co-assembled by Trz-$(Cbz)_3$ and Rh6G, a new emission peak appeared at 608 nm (Fig. 3c). The delayed emission spectrum (λ_{ex} = 328 nm, delay time = 5 ms) of 1D-SNRs showed a strong fluorescence afterglow band in the 525–750 nm range along with a relatively weak delayed fluorescence band at shorter wavelengths (400–500 nm range) (Fig. S6 in Supporting information). The emission peak at 554 nm in the phosphorescence mode originated from Trz-$(Cbz)_3$, while the emission peak at 608 nm overlapped with the fluorescence peak of Rh6G. It was reasonably inferred that the 608 nm peak was the long lifetime fluorescence peak of Rh6G through the TS-FRET process. The fluorescence afterglow band exhibited an ultralong average lifetime of 226 ms ($\lambda_{monitored}$ = 608 nm) with an excellent quantum yield (ϕ_P = 16.6%) in air (Fig. 3d). Additionally, visible red afterglow with remarkable ambient stability of the 1D-SNRs solid powders was evident from the photographs (Fig. 3e), indicating the delayed-fluorescence nature of the Rh6G emission originating from the long-lifetime triplet state of Trz-$(Cbz)_3$.

As noted previously, the new emission peak at 608 nm in the delayed emission spectrum of 1D-SNRs may be attributed to TS-FRET between Trz-$(Cbz)_3$ and Rh6G. In Förster theory, the spectral overlap between the donor and acceptor is a critical factor in energy transfer [38]. To investigate whether this process occurred, the absorption spectrum of Rh6G and the delayed emission spectrum of Trz-$(Cbz)_3$ were measured and analyzed. The absorption spectrum of Rh6G showed a characteristic band with a maximum at 551 nm, and Trz-$(Cbz)_3$ exhibited a phosphorescence emission with a maximum at 554 nm, indicating significant spectral overlap between them (Fig. 4a). To explore the TS-FRET process, gated emission spectra of 1D-SNRs with different amounts of Rh6G were analyzed.

The emission peak at 554 nm, attributed to Trz-$(Cbz)_3$, decreased gradually, while the emission peak at 608 nm, attributed to Rh6G, increased remarkably (Fig. 4b). This observation strongly suggests energy transfer processes, confirming the delayed sensitization of Rh6G by TS-FRET from Trz-$(Cbz)_3$. As a result, 1D-SNRs function as long-lived organic phosphors, exhibiting multi-color afterglow emission from yellow to red, with corresponding changes in CIE coordinates from (0.42, 0.58) to (0.62, 0.33) (Fig. S7 in Supporting information). Importantly, various assemblies with different ratios of Trz-$(Cbz)_3$ and Rh6G maintained their regular 1D nanorod structures (Fig. S8 in Supporting information). This finding provides valuable insights for designing phosphorescent materials with multiple luminescent colors. To further understand the TS-FRET process, the quenching of the donor's lifetime by the acceptor was analyzed. Time-resolved emission lifetime analyses of Trz-$(Cbz)_3$ revealed a gradual decrease in the average lifetime from 232 ms to 6.9 ms as the Rh6G content increased (Fig. 4c). Similarly, the lifetime of Rh6G monitored at 608 nm showed a corresponding decrease (Fig. 4d).

These decay profiles clearly indicate the efficient transmission of energy from the triplet states of Trz-$(Cbz)_3$ to the singlet states of Rh6G acceptors without radiation in 1D-SNRs [39]. The TS-FRET efficiency of 1D-SNRs was quantitatively estimated to be 97%, which surpasses the efficiency of most previously reported energy transfer systems [40]. And the antenna effect value was calculated to be 30.58. To further confirm that the long-lived emission peak at 608 nm results from sensitization of the singlet states *via* TS-FRET, emission spectra in the phosphorescence mode of 1D-SNRs were measured at 554 nm excitation wavelength. No long-lived emission peak at 608 nm was observed (Fig. S9a in Supporting information), only resulting in prompt fluorescence in the nanosecond timescale (3.6 ns) (Fig. S9b in Supporting information). This experimental evidence strengthens the conclusion that the emission at 608 nm in the phosphorescent spectrum of 1D-SNRs is indeed due to the sensitization of singlet states through TS-FRET. The temperature has a great influence on the fluorescence afterglow. As shown in Fig. S10 (Supporting information), on increasing the temperature from 300 K to 400 K, the delayed emission spectra and time-resolved emission decay of 1D-SNRs decreased ob-

viously. Such phenomenon is attributed to the energy of molecular vibrations and nonradiative loss increased with increasing temperature.

To elucidate the TS-FRET process occurring between Trz-$(Cbz)_3$ and Rh6G within 1D-SNRs, the electronic structure and energy level were investigated using time-dependent density functional theory (TD-DFT) calculations. As indicated in Fig. S11 (Supporting information), Trz-$(Cbz)_3$ exhibits multiple Tn values, with $T_2 \sim T_6$ either above or below the S_1 energy level at 0.3 eV, thereby enabling two channels ($S_1 \rightarrow T_6$ and $S_1 \rightarrow T_5$) to partake in the efficient ISC process, ensuring the phosphorescent emission of Trz-$(Cbz)_3$, the k_r of Trz-$(Cbz)_3$ is $2.91672432 \times 10^{-5}\ s^{-1}$, and the τ_{ISC} is 3.43 ns. Additionally, the $T_1 \sim T_6$ values are higher than those of S_1 in Rh6G, which permits the possibility of engendering TS-FRET between them. Furthermore, molecular mechanics calculations revealed that the intermolecular distance between Trz-$(Cbz)_3$ and Rh6G is 3.6 Å, a distance within the range (typically 10–100 Å) at which FRET occurs [41], thereby providing theoretical support for the realization of the TS-FRET process (Fig. S12 in Supporting information). Based on the experimental and theoretical findings, a plausible energy-transfer mechanism for 1D-SNRs (Fig. 1b) is proposed, whereby Trz-$(Cbz)_3$ absorbs UV excitation light (328 nm) and undergoes a ground state transition to the excited singlet states S_1. Subsequently, S_1 states undergo intersystem crossing to the excited triplet states T_n, leading to yellow phosphorescence emission at 554 nm. Trz-$(Cbz)_3$ has multiple T_n values that are higher than the S_1 of Rh6G. Therefore, the triplet excited state energy can be effectively transferred to the singlet excited state between them. Due to the effective restriction of non-radiative transition of rigid environment in one-dimensional nanorods, more energy emits fluorescence and shows afterglow phenomenon when S_1 transitions back to S_0.

Based on the above results, we put forward a hypothesis that the formation of cation-π interactions between Trz-$(Cbz)_3$ and Rh6G is a crucial factor in enhancing TS-FRET. To test this hypothesis, we conducted a series of experiments to confirm the existence of cation-π interactions in 1D-SNRs. In ^{1}H NMR titration spectra (Fig. 5a), the peak related to protons Ha of carbazolyl in Trz-$(Cbz)_3$ underwent upfield shifts with the gradual addition of Rh6G, indicating the complexation of N^+ with the carbazolyl moiety. Fluorescence emission spectra experiments (Fig. 5b) in solution showed that the cation-π complexes show a new emission peak at 576 nm, which gradually enhanced with the addition of Rh6G to the Trz-$(Cbz)_3$ solution. Furthermore, the solid-state ^{13}C NMR spectra (Fig. 5c) demonstrated clearly upfield of the C_a next to the N^+ cation in Rh6G due to the higher shielded environment of carbazole. However, the N^+–carbazole interaction cannot cause large perturbations to the electronic structure of ethyl in the Rh6G, only a small downfield shift of C_1 and C_2 of ethyl group. This result further confirmed the existence of strong cation-π interactions between Trz-$(Cbz)_3$ and Rh6G in the 1D-SNRs. Raman spectra analysis (Fig. 5d) showed that the absorption peaks around 1187 and 1308 cm^{-1} represent breathing mode and out-of-plane bending of benzene rings in Trz-$(Cbz)_3$. The value of I_{1187}/I_{1308} decreases from 1.072 to 0.969 with and without Rh6G, implying that the vibration mode of carbazole rings in Trz-$(Cbz)_3$ is changed due to the cation-π interaction. Non-covalent interaction (NCI) and DFT calculation analysis of monomers and 1D-SNRs provided further evidence for the cation-π interaction between Trz-$(Cbz)_3$ and Rh6G. As shown in Figs. 5e and f, the NCI shows a yellow-green bowl area in the 3D space between N^+ and carbazole, belonging to the cation-π interaction between them. The optimized conformation that the interaction strength between Trz-$(Cbz)_3$ and three Rh6G molecules (−71.01 kcal/mol) is greater than that between Trz-$(Cbz)_3$ dimer (−41.09 kcal/mol) (Fig. S13 in Supporting information). Taken together, these results provide strong evidence for the existence of

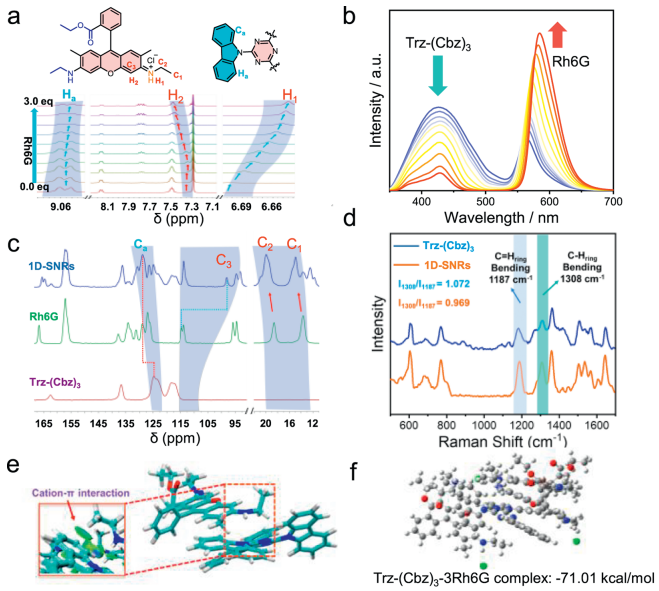

Fig. 5. Confirmation of the existence of strong cation-π interactions in 1D-SNRs. (a) Partial ^{1}H NMR spectra recorded (400 MHz, 298 K, $CDCl_3$). (b) Fluorescence titration of individual Trz-$(Cbz)_3$ (5.0 mmol/L) in $CHCl_3$ in the presence of 0–3.0 equiv. of Rh6G concentrations ($\lambda_{ex} = 328$ nm). (c) Solid-state ^{13}C NMR spectra of Trz-$(Cbz)_3$ (top), 1D-SNRs (middle) and Rh6G (bottom); (d) Raman spectrum of Trz-$(Cbz)_3$ (top) and 1D-SNRs (bottom). (e) Noncovalent interaction (NCI) analysis of the complexes of Trz-$(Cbz)_3$ and Rh6G. (f) DFT optimized structures and interaction energies of Trz-$(Cbz)_3$–3Rh6G complexes.

cation-π interactions in 1D-SNRs and suggest that this interaction is a key factor in enhancing TS-FRET.

Besides, we aimed to investigate the role of cation-π interactions in enhancing the dipole-dipole interaction between Trz-$(Cbz)_3$ and Rh6G within 1D-SNRs and leading to efficient TS-FRET. For this purpose, we performed density functional theory (DFT) calculations and molecular dynamics (MD) simulations to gain insight into the molecular organization of 1D-SNRs. The MD simulations revealed that the Rh6G molecules form a helical packing arrangement around the Trz-$(Cbz)_3$ monomers (Fig. 6a), which is consistent with the ordered helical organization observed in electron microscopy results (Fig. 2). During the MD trajectory, we studied the impact of the structural organization of donors and acceptors on the macro-dipole moment. As shown in Figs. 6a-c, the mean macro-dipole moment for 1D-SNRs (5.43 D) is found to be significantly higher than that of Trz-$(Cbz)_3$ (0.03 D). This enhancement in the dipole moment is attributed to the significant increase in dipole moments caused by the asymmetry of the positions of the electron cloud, resulting from the cation-π interactions between Trz-$(Cbz)_3$ and Rh6G. Consequently, this leads to an intensified dipole-dipole interaction along the twisted helix, which is beneficial for efficient TS-FRET. To further support this observation, we performed DFT calculations to map the electrostatic potential (ESP) surfaces, which describe the asymmetric distribution of electron clouds. In the ESP mapping of Trz-$(Cbz)_3$ (Fig. S14 in Supporting information), negative charge is delocalized in the carbazole group, while triazine acts as an acceptor and stabilizes the negative charge, resulting in a small dipole moment (0.0027 debye). However, when considering the cation-π dimer, the dipole moments were found to be as large as 5.3725 debye, indicating a significant enhancement in the dipole-dipole interactions due to cation-π interactions, which accelerates TS-FRET substantially. Moreover, the orientations of the dipoles of Trz-$(Cbz)_3$ and Rh6G can be adjusted to a suitable arrangement where their dipole moments are helically aligned along the central axis

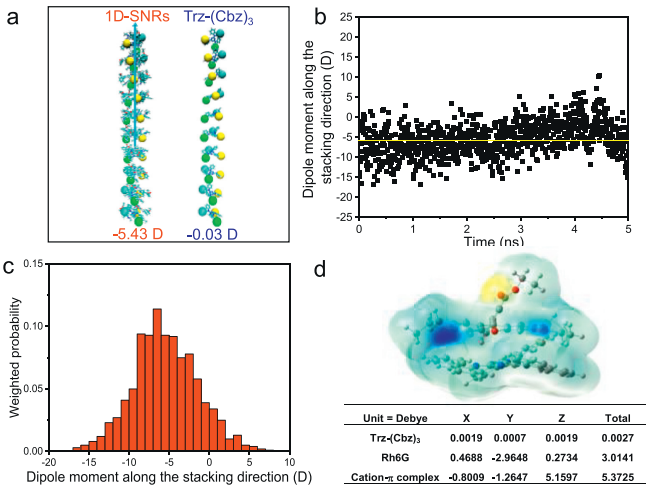

Fig. 6. Cation-π interactions enhanced dipole-dipole interactions confirmed by theoretical calculations. (a) Snapshot illustrating the arrangement of molecules in the assembled state. Linkers are highlighted in yellow, blue and cyan to aid in the visualization of the helical packing. (b) Macro-dipole along the stacking direction as a function of time. Solid horizontal line is drawn to represent the mean dipole moment value for the system. (c) Weighted probability distribution of macro-dipole obtained from (b). (d) Electrostatic potentials (ESP) mapped onto the electron density surfaces ($\delta = 0.01$) (top view) calculated at the B3LYP/6–31+G(d, p) level for stacking structures of donor-acceptor complex (up) and the calculation of dipole moment of Trz-$(Cbz)_3$, Rh6G and cation-π complex (below).

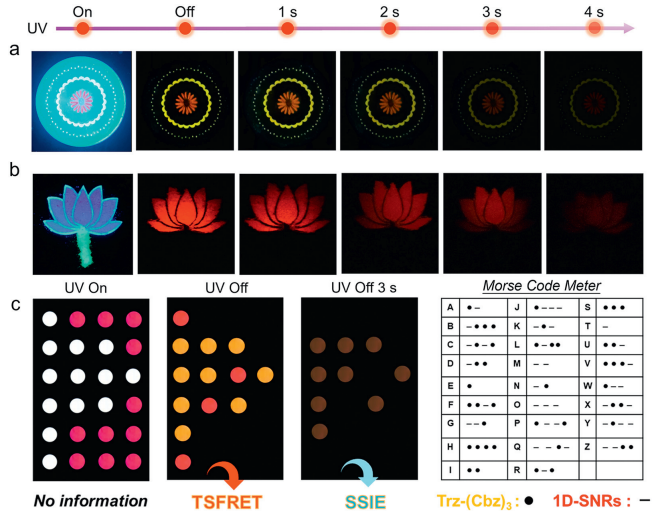

Fig. 7. Application of 1D-SNRs in information encryption. (a, b) Schematic diagram of some patterns of writing with 1D SNRs as filler before and after UV light and at different time intervals after removing the UV light. (c) Appearances of multimodal optical signals in Morse code of 1D-SNRs. The outer yellow circle and wreath are the Trz-$(Cbz)_3$ and internal red flowers for the 1D-SNRs in (a); In (b), the red lotus part is the 1D-SNRs, and the root part is anthracene; The red dots in (c) represent the 1D-SNRs and the yellow dots represent the Trz-$(Cbz)_3$.

Table 1
Photophysical parameters and TS-FRET properties of assemblies based different cationic dyes with good spectral overlap with the Trz-$(Cbz)_3$.

Cations	λ_{abs} (nm)	λ_{FA} (nm)	ϕ_P (%)[a]	τ_P (ms)[b]	E (%)[c]
Rh6G	551	608	16.5	226	97
Eosin B	598	617	9.2	213	92
Congo Red	519	621	7.5	209	90
Acid Blue 93	521	648	6.8	216	93
Acid Red 27	503	619	4.9	202	87

[a] ϕ_P is quantum yield.
[b] Triplet lifetime of the assemblies based different cationic dyes with Trz-$(Cbz)_3$.
[c] TS-FRET efficiency (E) of the assemblies according to the equation $E = 1 - \tau_{DA}/\tau_D$.

of 1D-SNRs, promoting a successful energy transfer process [42]. To investigate the role of the cation component in influencing the TS-FRET process, we designed a structure control experiment. In this experiment, monomers Trz-$(Cbz)_3$ and Rh6G-2, without the N^+ cation, were assembled under the same conditions. However, no regular assembly morphology was observed, and the phosphorescence spectrum only exhibited 554 nm, indicating that no energy transfer occurred (Fig. S15 in Supporting information). Theoretical calculations and control experiment results collectively demonstrated that the cation-π interaction is indeed responsible for the enhanced TS-FRET within 1D-SNRs.

In addition to investigating the cation-π enhanced TS-FRET between Trz-$(Cbz)_3$ and Rh6G, we aimed to demonstrate the universality of this phenomenon through a series of control experiments. To achieve this goal, we constructed supramolecular assemblies using other typically cationic dyes that exhibit good spectral overlap with Trz-$(Cbz)_3$. The selected dyes included Eosin B, Congo Red, Acid Blue 93 and Acid Red 27. The photophysical parameters of these assemblies were investigated and presented in Table 1 and Figs. S16-S19 (Supporting information). The results indicated that the cation-π enhanced TS-FRET has a wide range of applicability across these systems due to the existence of cation-π enhanced dipole-dipole interactions. Among these cationic dyes, 1D-SNRs based on Rh6G showed the highest energy transfer efficiency, primarily due to its highest spectral overlap with the Trz-$(Cbz)_3$ triplet emission. As the overlap area of absorption spectra of these cationic dyes and the emission spectrum of Trz-$(Cbz)_3$ decreased gradually, we observed a decrease in the corresponding energy transfer efficiency. Moreover, the afterglow wavelength (λ_P) and lifetime (τ_P) of 1D-SNRs can be tuned by changing the kind of cationic dyes used. This finding offers valuable insights into the design and application of cation-π enhanced TS-FRET in various systems, providing a versatile approach to achieve efficient energy transfer between donor and acceptor molecules.

Room temperature phosphorescent and fluorescence afterglow materials have great application prospects in the field of information encryption [43–50]. Therefore, after elucidating the mechanism for efficient TS-FRET emission in the 1D-SNRs system, we explored their potential applications, particularly in the field of information encryption. The ease of preparation of 1D-SNRs as solid powders with good thermal and air stability (Fig. S20 in Supporting information) and solvent tolerance (Fig. S21 in Supporting information) makes them highly promising as stuffing materials for mould used in information encryption. In Fig. 7, we demonstrate the application of 1D-SNRs in creating visually distinct patterns using 3D-printed mould. By filling the mould with Trz-$(Cbz)_3$ and 1D-SNRs, we can create intricate shapes with different colors under natural and UV lights. For instance, a mould with a surrounding wreath of Trz-$(Cbz)_3$ and an inner flower core comprising 1D-SNRs creates a blue flower appearance under UV light. Upon cessation of the 365 nm UV excitation, the surrounding wreath and inner flower core emit yellow and red afterglow, respectively, which can be easily distinguished by the naked eye and lasts for several seconds due to the ultralong RTP lifetime of Trz-$(Cbz)_3$ and 1D-SNRs. Additionally, we demonstrated the use of 1D-SNRs with a fluorescent molecule, anthracene, as an interference agent in a 3D-printed lotus flower with a stem. By filling the stem with anthracene and the flower with 1D-SNRs, a blue-lotus flower with a green stem pattern is visible under 365 nm excitation. However, upon cessation of the 365 nm lamp, the green stem immediately disappears, and the number of petals in the red lotus flower gradually decreases over time due to the ultra-long afterglow lifetimes of 1D-SNRs (Fig. 7b). Furthermore, luminescent Morse code patterns were prepared by adding 1D-SNRs and Trz-$(Cbz)_3$ to the printed

containers, with red representing "underscore" and yellow representing "dot" (Fig. 7c). During the encryption process (UV on), the Morse code is not visible, displaying "No information." However, upon removal of the UV lamp, obvious afterglow emissions reveal the first encryption message "TSFRET." After 3.0 s of UV light removal, the pattern transforms into another new encryption message "SSIE". These experiments demonstrate that 1D-SNRs have significant potential for use in the field of phosphorescent anti-counterfeiting and information encryption. The versatility of 1D-SNRs and their unique afterglow properties open up exciting possibilities for various applications, including security materials, anti-counterfeiting measures, and information encryption, where their long-lived luminescence and tunable colors can add value and efficiency to these technologies.

In summary, we present a successful cation-π enhanced TS-FRET strategy using 1D nanorods matrix. By co-assembly of a long-lived organic phosphor Trz-$(Cbz)_3$ and a commercially available fluorescent dye Rh6G, the efficiency of TS-FRET reaches a high of 97%, resulting in delayed sensitization of Rh6G singlet and afterglow luminescence. The effectiveness of the cation-π interactions on the dipole moments of Trz-$(Cbz)_3$ and Rh6G along the stacking direction of 1D-SNRs was demonstrated by a series of experimental data and theoretical calculation results. The wavelength of TS-FRET could be easily tuned by selecting appropriate acceptor dyes, indicating that the cation-π enhanced TS-FRET has broad applicability. Furthermore, the afterglow luminescence resulting from the cation-π enhanced TS-FRET exhibited clear photos by camera, making it a promising candidate for anti-counterfeiting applications and information encryption. Our findings offer a generalized strategy for enhancing TS-FRET through the regulation of the ordered arrangement and dipole-dipole interaction of donor and acceptor.

Declaration of competing interest

The authors declare that they have no known competing financial interests or personal relationships that could have appeared to influence the work reported in this paper.

CRediT authorship contribution statement

Shuai Qiu: Writing – original draft. **Jia He:** Data curation. **Xiao Hu:** Software. **Hongxia Yan:** Formal analysis. **Zhao Gao:** Data curation. **Wei Tian:** Writing – review & editing, Project administration.

Acknowledgments

This work was financially supported by the National Natural Science Foundation of China (Nos. 22071197, 22022107), Key Research Program of Frontier Sciences, CAS (No. QYZDJ-SSW-SLH044), Key Research Program of the Chinese Academy of Sciences, (No. XDPB01), Fundamental Research Funds for the Central Universities (No. D5000230114) and China Postdoctoral Science Foundation (No. 2023M730951).

Supplementary materials

Supplementary material associated with this article can be found, in the online version, at doi:10.1016/j.cclet.2024.110057.

References

[1] T. Förster, Naturwissenschaften 6 (1946) 166–175.
[2] L. Wu, C. Huang, B.P. Emery, et al., Chem. Soc. Rev. 49 (2020) 5110–5139.
[3] A.J.P. Teunissen, C.P. Medina, A. Meijerink, et al., Chem. Soc. Rev. 47 (2018) 7027–7044.
[4] L. Mendive-Tapia, M. Vendrell, Acc. Chem. Res. 55 (2022) 1183–1193.
[5] X. Wang, Z. Gao, W. Tian, Chin. Chem. Lett. 35 (2024) 109757.
[6] Y. Li, C. Xia, R. Tian, et al., ACS Nano 16 (2022) 8012–8021.
[7] P. Jia, Y. Hu, Z. Zeng, Y. Wang, et al., Chin. Chem. Lett. 34 (2023) 107511.
[8] C. Lin, P. Han, S. Xiao, et al., Adv. Funct. Mater. 31 (2021) 2106912.
[9] A. Cravcenco, M. Hertzog, C. Ye, et al., Sci. Adv. 5 (2019) eaaw5978.
[10] Y. Zhao, L. Ma, Z. Huang, et al., Adv. Optical Mater. 10 (2022) 2102701.
[11] Y. Tian, J. Yang, Z. Liu, et al., Angew. Chem. Int. Ed. 60 (2021) 20259–20263.
[12] M. Kanakubo, Y. Yamamoto, Y. Kubo, Bull. Chem. Soc. Jpn. 94 (2021) 1204–1209.
[13] Y.Y. Hu, X.Y. Dai, X. Dong, et al., Angew. Chem. Int. Ed. 61 (2022) e202213097.
[14] X. Cui, W. Shi, C. Lu, J. Phys. Chem. A 125 (2021) 4209–4215.
[15] F. Lin, H. Wang, Y. Cao, et al., Adv. Mater. 34 (2022) 2108333.
[16] S. Kuila, S.J. Georg, Angew. Chem. Int. Ed. 59 (2020) 9393–9397.
[17] S. Garain, B.C. Garain, M. Eswaramoorthy, et al., Angew. Chem. Int. Ed. 60 (2021) 19720–19724.
[18] R. Gao, D. Yan, Chem. Sci. 8 (2017) 590–599.
[19] Y. Mu, B. Xu, Z. Yang, et al., ACS Appl. Mater. Interfaces 12 (2020) 5073–5080.
[20] A. Cravcenco, C. Ye, J. Gräfenstein, et al., J. Phys. Chem. A 124 (2022) 7219–7227.
[21] F.F. Shen, Y. Chen, X. Dai, et al., Chem. Sci. 12 (2021) 1851–1857.
[22] M. Huo, X.Y. Dai, Y. Liu, Adv. Sci. 9 (2022) 2201523.
[23] H. Gui, Z. Huang, Z. Yuan, et al., CCS Chem. 3 (2021) 481–489.
[24] X. Zhong, T. Chervy, S. Wang, et al., Angew. Chem. Int. Ed. 55 (2016) 6202–6206.
[25] D. Dovzhenko, M. Lednev, K. Mochalov, et al., Chem. Sci. 12 (2021) 12794–12805.
[26] O. Erdem, K. Gungor, B. Guzelturk, et al., Nano Lett. 19 (2019) 4297–4305.
[27] A. Iqbal, S. Arslan, B. Okumus, et al., Proc. Natl. Acad. Sci. U. S. A. 105 (2008) 11176–11181.
[28] G. Jiang, J. Yu, J. Wang, et al., Aggregate 3 (2022) e285.
[29] S. Garain, S.M. Wagalgave, A.A. Kongasseri, et al., J. Am. Chem. Soc. 144 (2022) 10854–10861.
[30] H.T. Chifotides, K.R. Dunbar, Acc. Chem. Res. 46 (2013) 894–906.
[31] X. Xiao, H. Chen, X. Dong, et al., Mater. Chem. Front. 6 (2022) 3261–3270.
[32] Z. Gao, L. Shi, F. Yan, et al., Angew. Chem. Int. Ed. 62 (2023) e202302274.
[33] H. Huo, X. Xiao, L. Chang, et al., Sci. China Chem. 66 (2023) 2070–2082.
[34] G. Zhao, H. Zhu, Adv. Mater. 32 (2020) 1905756.
[35] J. Kang, J. Yu, A. Li, et al., iScience 15 (2019) 119–126.
[36] A. Turupcu, J. Tirado-Rives, W.L. Jorgensen, J. Chem. Theory Comput. 16 (2020) 7184–7194.
[37] X. Xiao, H. Chen, X. Dong, et al., Angew. Chem. Int. Ed. 59 (2020) 9534–9541.
[38] W.C. Geng, Z. Ye, Z. Zheng, et al., Angew. Chem. Int. Ed. 60 (2021) 19614–19619.
[39] R.G. Bennett, R.P. Schwenker, R.E. Kellogg, J. Chem. Phys. 41 (1964) 3040–3041.
[40] P.P. Jia, L. Xu, Y.X. Hu, et al., J. Am. Chem. Soc. 143 (2021) 399–408.
[41] L. Wu, C. Huang, B.P. Emery, et al., Chem. Soc. Rev. 49 (2020) 5110–5139.
[42] H. Liu, H. Fu, X. Shao, et al., J. Chem. Theory Comput. 16 (2020) 6397–6407.
[43] B. Zhou, Z. Qi, M. Dai, et al., Angew. Chem. Int. Ed. 62 (2023) e202309913.
[44] T. Wang, M. Liu, J. Mao, et al., Chin. Chem. Lett. 35 (2024) 108385.
[45] L. Zheng, K. Jiang, J. Du, et al., Chin. Chem. Lett. 34 (2023) 107950.
[46] C. Xing, B. Zhou, D. Yan, et al., CCS Chem. 5 (2023) 2866–2876.
[47] C. Xing, Z. Qi, B. Zhou, et al., Angew. Chem. Int. Ed. (2024) e202402634.
[48] C. Xing, B. Zhou, D. Yan, et al., Adv. Sci. 11 (2024) 2310262.
[49] Y. Wu, X. Fang, J. Shi, et al., Chin. Chem. Lett. 32 (2021) 3907–3910.
[50] X. Wang, Z. Chen, J. Yin, et al., Chin. Chem. Lett. 33 (2022) 2522–2526.